Chapter – 5

Spectroscopy of Nuclei around Proton Shell Closures: Structure of ^{36}Cl and ^{54}Mn

5.1. Introduction

The configurations of low-lying high spin states in nuclei near closed shells are expected to be rather pure. The excitation spectra in the low-energy region for these nuclei show irregular and complex patterns, typically for near-spherical nuclei and are dominated by single- and multi-particle excitations. Spectroscopic information on these levels provide important avenues to the empirical single particle energies and the residual N-N interactions needed for understanding nuclear structure in the shell model framework. The study of odd-odd nuclei offers a scope for investigating the underlying proton-neutron residual interaction. Such nuclei exhibit highly complex level structure because of a large number of possible coupling of the odd proton to the even-even core.

The odd-odd nuclei ^{36}Cl with 17 protons and 19 neutrons is a subject of much interest for many years due to its closeness to doubly magic structure (Z = N = 20). The previously known complex nature of the level structure and their spectra depicts the near spherical nature of the nucleus in the low lying states which is mainly dominated by single particle excitations. The study of odd-odd nuclei such as ^{36}Cl offers a scope for investigating the underlying proton-neutron residual interactions.

For nuclei above mass A = 40 the N = Z line drifts more and more away from the line of stability with increasing mass of the nuclei. Together with a rather small Coulomb barrier gives rise to an interesting aspect of the heavier N ~ Z nuclei, namely the proton, alpha, or even cluster emission may play a role in the decay of their excited states. Generation of angular momentum in nuclei in the vicinity of ^{54}Mn have drawn considerable interest, both experimentally and theoretically, due to their proximity to the proton and neutron shell closure at Z = N ~ 28 respectively.

5.2. Literature Survey

5.2.1. Spectroscopy of Odd-Odd Nucleus ^{36}Cl

The nucleus ^{36}Cl was earlier studied by several authors mainly by light particle induced reactions followed by γ-γ coincidence measurements using two coaxial Ge(Li) detectors [1 - 8]. These studies have extended the level structure of ^{36}Cl up to excitation energy of ~ 5 MeV. Spin and parity of the levels were determined using the angular distributions and linear polarization methods [4, 5]. Life time measurements have been performed by the recoil distribution method (RDM) [4]. It was found that the levels in ^{36}Cl found by Nolan

et al., [4] had lifetimes and decay schemes characteristic of the $J^{\pi} = 5^-$ and 4^- levels predicted in the shell-model calculations of Erné *et al* [9].

The motivation behind the study by Keinonen *et al.,* [10] was to study the γ-decay of 5.31 MeV (7^+ state) in ^{36}Cl and the M2 strength of the 5.31 → 2.52 MeV ($7^+ \rightarrow 5^-$) transition. It is noted that the ^{36}Cl offers a rare feature of two successive stretched M2 transitions, as the 2.52 MeV (5^- state) decays via M2 to the 0.79 MeV (3^+ state). The article by Keinonen *et al.,* [10] which employed the reaction $^{25}Mg(^{18}O, \alpha p)^{36}Cl$, observed three transitions of 1019-, 1776- and 2795-keV apart from the states up to 2811-keV [5,11]. These observed transitions were attributed to the decay of states at 5313- and 4294-keV excitation energy. Spin and parity assignments of the 4.29 MeV level are based on the angular distribution measurements and on comparison with the previous works [5, 6, 12].

The γ-ray decays of high-spin states in ^{36}Cl was studied via heavy ion induced fusion reactions involving ^{14}N bombardment on target of ^{27}Al [13]. Decay schemes and spin-parity assignments were deduced from γ-γ coincidence measurements, γ-ray angular distribution, linear polarization measurements to establish the spin-parities of the observed levels. To measure the life times, they have used the recoil-distance method (RDM). They have observed all the levels below 4 MeV which were well studied earlier. The 4294- and 5313-keV levels which we found were also observed by Rascher *et al.,* [14] *via* fusion evaporation reactions and the 5313-keV level had been observed by Sherr *et al.,* [6]. They have suggested a level at 5.78-keV which if present is likely to be $J = 8$ state. The weak coupling predictions would then suggest $J^{\pi} = 8^+$ state.

The radiation emitted after thermal neutron capture γ-ray measurements in ^{36}Cl has been extensively studied. The nucleus ^{36}Cl has also been investigated previously with different types of pick-up and stripping reactions and with neutron capture γ-ray measurements [15 - 20]. All these works enhanced the knowledge on the structure of ^{36}Cl.

5.2.2. Spectroscopy of Odd-Odd Nucleus ^{54}Mn

A variety of physics of the odd-odd nuclei has been studied in the mass A ~ 50 region [21 - 24]. Smooth band termination was observed by BaoGuo *et al.* [25], in the odd-odd nuclei ^{46}V and ^{50}Mn. Both these nuclei are normally deformed with no sign of shape coexistence within the same configuration. There is no existing data on the next odd-odd

nuclei such as ^{52}Mn, ^{54}Mn which shows band termination. The odd-odd ^{54}Mn nucleus, with 25 protons and 29 neutrons, has been earlier studied both experimentally and theoretically and it has been found that the low-lying excitation spectra up to ~ 3.9 MeV and J ~ 8$\hbar$ are irregular, originating from single- and multiparticle excitations. A number of such low-lying states have been identified earlier by in-beam studies [26 - 39].

The reactions leading to the nuclei ^{54}Mn have been studied by using proton capture [26 - 28] in the past. Ogawa *et al.*,[26] has studied the excitation functions and angular distributions of γ-rays in the reaction ^{54}Cr(p, nγ)^{54}Mn in order to establish the spins and parities of levels in ^{54}Mn. Using the theoretical predictions of the statistical compound-nucleus model, unique spin assignments were obtained up to the level 1009.9-keV. In the other reactions involving proton capture studies, Kerr *et al.*, [27] has studied the angular distribution and g-factor measurements upto 1072-keV level of ^{54}Mn. Beale *et al.*, [28] has used the Doppler shift attenuation method (DSAM) used to deduce the lifetimes up to 2354-keV level. The decay of nuclei leading to the nuclei ^{54}Mn has been studied through various reactions [29, 31]. Beuzit *et al.*,[29] studied the particle-gamma-ray coincidences from the ^{58}Ni(p, p'γ) reaction at 12 MeV. The major decay modes of the levels up to 8.11 MeV of excitation energy were determined. In the reaction by Betts *et al.*, [30], the level scheme of ^{54}Mn has been studied by means of the ^{52}Cr(τ, p) reaction at incident energies of 15 and 16.5 MeV. Levels up to 7 MeV of excitation have been measured. Majumder *et al.*, [31] has studied the (d, *) reaction in ^{56}Fe at energy E_d = 12 MeV and angular distributions of the *-particles are obtained over the angular range 13°–83° (c.m.s.); The results were analysed in terms of the DWBA theory, spectroscopic information on ^{54}Mn levels upto 4.3 MeV of excitation was obtained.

In the reactions ^{51}V(^{7}Li, *p3n*)^{54}Mn, ^{51}V(^{6}Li, *p2n*)^{54}Mn by Poletti *et al.*, [32] at about 25 MeV of beam energy, they have assigned the γ-rays to the decay of 5 higher lying levels between 1461- and 2856-keV. Most of the γ-rays observed from the γ-γ coincidence and γ-ray singles measurements were observed by Ogawa and Taketani *et al.*, [26]. Lifetime measurements were performed using the Recoil Distance Method (RDM). Life time of 156-, 368- and 1073-keV levels measured using RDM method. Nathan *et al.*, [33] have used the fusion-evaporation reactions induced by a beam of 35 MeV ^{11}B on isotropically enriched ^{48}Ca target to populate high-spin states in ^{54}Mn. Their measurements consisted of γ-ray excitation functions, angular distributions, γ-γ coincidences, recoil distance and Doppler shift lifetime measurements. From the above

measurements they have deduced the energy levels, γ-ray branching ratios, spin-parity assignments and life times. On the other hand Poletti *et al.,* [32] have used recoil distance method (RDM), γ-γ coincidence measurements, angular distribution measurements and Doppler shift attenuation life time measurements (DSAM) to study this even mass nucleus ^{54}Mn. They have observed several γ-rays out of which only four most intense γ-rays were observed by Nathan *et al.,* [33]. The main contribution is a more accurate lower limit on the life time of the 156-keV level.

Radford *et al.,*[34] has performed the recoil-distance method (RDM) to be used in conjunction with the ^{51}V(α, n) reaction to investigate the lifetimes of four levels in ^{54}Mn. In addition, Doppler-shift attenuation method was used to investigate more lifetimes in ^{54}Mn. The mean lifetimes of 156-, 368-, 408- and 1073-keV were measured by RDM. The centroids in γ-ray angular distribution studies have been used to obtain DSAM measurements of the mean lives of levels in ^{54}Mn. The RDM results in ^{54}Mn are in good agreement and have resulted in much more accurate knowledge of the mean lives. High-spin states in ^{54}Mn were populated in the ^{52}Cr(α, pnγ) reaction by Toulemonde *et al.,* [35]. They have used the angular distribution, linear polarization and γ-γ coincidence measurements to assign the spin-parity of the 1073-, 1784-, 1925-, 2857-, 3244-keV levels and in addition to that they have found a new level at 3939-keV.

Comparison of experimental results with shell-model calculations for ^{54}Mn was given by some authors [32, 33]. The nuclei with N=29 and Z=20 ~ 28 were described by the shell model, assuming $(1f_{7/2})^{Z-20}$ configuration for protons and $(2p_{3/2}, 2p_{1/2}, 1f_{5/2})^1$ for one neutron outside the ^{48}Ca core [36]. Effective two-body matrix elements between the $1f_{7/2}$ - proton and $(2p_{3/2}, 2p_{1/2}, 1f_{5/2})$ - neutron are determined by a least-square fitting to the observed level energies of the N = 29 isotones. Poletti *et al.,* [32], Nathan *et al.,* [33] have compared their experimental results with that of the Horie and Ogawa [36]. Their theoretical calculations show quite reasonable energy agreement for the lowest few excited states with the experimentally determined ones. However they fail to predict the long-lived levels in ^{54}Mn. Kerr *et al.,* [37], Guichard *et al.,* [38] have suggested that the levels be based on the excitation of one of the $f_{7/2}$ neutrons to higher orbitals on the basis of lifetimes. The first calculations to include the 2-particle-4-hole excitations are those by Johnstone and Benson [39]. Their agreement with the experiment in case of ^{54}Mn is impressive. They have calculated the excitation energies of states belonging to various n_1 - particle - n_2 - hole (n_1P - n_2h) configurations relative to the ^{56}Ni Core. They have

predicted that the first 6^+ state, which they associated with the 1073-keV level, is an intruder state having a 2p-4h configuration.

5.3. Aim of the Present work

The level structure of the odd-odd ^{36}Cl is expected to be interesting due to the proximity of both the proton and neutron numbers to the Z, N ~ 20 shell closure. Information on the level structure of this nucleus is available from single-neutron stripping and pickup reactions [3], and hence is limited to moderate spins and excitation energy. It would be of interest to explore the level scheme to higher spin regimes, where one could expect configurations originating from nucleon excitations from the (2s,1d) shell into the (1f,1p) shell. Further the availability of a reasonable number of valence nucleons outside the core could result in the occurrence of deformed structure at high spins in this nucleus. In present work, the high spin states in ^{36}Cl were populated using the $^{20}Ne + ^{27}Al$ reaction.

The level structure of the odd-odd nuclei ^{54}Mn is populated mainly through proton capture and light heavy ions such as ^{4}He, $^{6,7}Li$, ^{11}B etc. Different investigations have been carried out by Poletti *et al.* [32], Nathan *et al.* [33], Radford and Poletti [34], Toulemonde *et al.*, [35] to study the level structure of ^{54}Mn up to an excitation energy of E_x ~ 4 MeV and spin-party of $J^\pi \sim 8^+$, using different techniques. We have employed the reaction $^{20}Ne + ^{51}V$ at an incident beam energy of 145 MeV to facilitate the above mentioned calculations. An attempt has been done to study the nucleus ^{54}Mn to explore the possibility of any shape changes due to the break-up of alpha cluster from the ^{20}Ne beam. The present work was initiated with the motivation to extend the level structure of ^{54}Mn to higher spins and to have a clear picture of the low-lying spectra of ^{54}Mn. The preliminary results from this investigation were presented earlier [40]. As expected, the low-lying spectra of ^{54}Mn (with Z = 25, N = 29) are irregular showing the single-particle character. With the addition of 10 new γ-transitions the level structure of ^{54}Mn has been extended up to excitation energy E_x ~ 5 MeV and $J^\pi = 15^+$.

5.4. Experimental Details

The experiment was carried out using the Indian National Gamma Array (INGA) [41] facility at Variable Energy Cyclotron Centre (VECC), Kolkata. The ^{36}Cl nucleus was populated using the $^{27}Al(^{20}Ne, n2\alpha2p)^{36}Cl$ reaction at a beam energy of 145 MeV. The delivered beam has a charge state of 6^+. A self-supporting ^{27}Al target of thickness ~

600μg/cm^2 was prepared by rolling Aluminium metal foil for the experiment. A Faraday cup is used to check the alignment of the beam falling on the target. It is placed just before the target chamber. The gamma rays emitted from the residual nuclei were detected using the Indian National Gamma Array (INGA) [41] facility consisting of six Compton-suppressed Clover detectors placed at 40°, 90°, and 125° with respect to the beam direction. The coincidence data was then gain matched to 1keV/channel and sorted into a 2-fold γ-γ symmetric and asymmetric (angle dependent) matrix. Data was taken for 12 shifts in which we have accumulated ~ 20 million coincidence counts.

Energy levels of ^{54}Mn were populated using the ^{20}Ne + ^{51}V reaction at incident beam energy of 145 MeV. The target consisted of a self-supporting ^{51}V foil of ~10 mg/cm^2 thickness which was rolled from metal foils. The INGA detector system employed for these measurements comprised of 8 Compton-suppressed Clover detectors. These detectors were placed two each at 40° (forward) and 125° (backward), four at 90° with respect to the beam direction. The master trigger was generated by a coincidence condition in which three or more Clover detectors had fired. Data was collected in 18 shifts (6 days). In all about 80 million three- or higher- fold coincidence events were accumulated in the list mode data.

A systematic procedure has been adopted for detailed off-line analysis of the acquired data. During the pre-sorting of the acquired data, instrumental drifts, if any, were corrected for. The add-back spectra were obtained after appropriate gain matching. Higher fold data were un-folded into the corresponding two-fold events. From this data the conventional E_γ-E_γ histograms (symmetric as well as angle-dependent) were generated. The pre-sorting as well as the sorting of the data were performed using the RADWARE [42] and IUCSORT [43] gamma analysis packages.

5.5. Results and Discussion

5.5.1. Level Structure of ^{36}Cl

All the previously observed transitions [4, 5, 13] have been observed. Fig. 5.1 illustrates the level structure of the nucleus ^{36}Cl. The newly found γ-transitions were marked with an asterisk (*). The level scheme is extended to an excitation energy of 7.5 MeV with the addition of more than 15 new transitions. They were placed in the level scheme carefully using the coincidence measurements (see Fig. 5.1.).

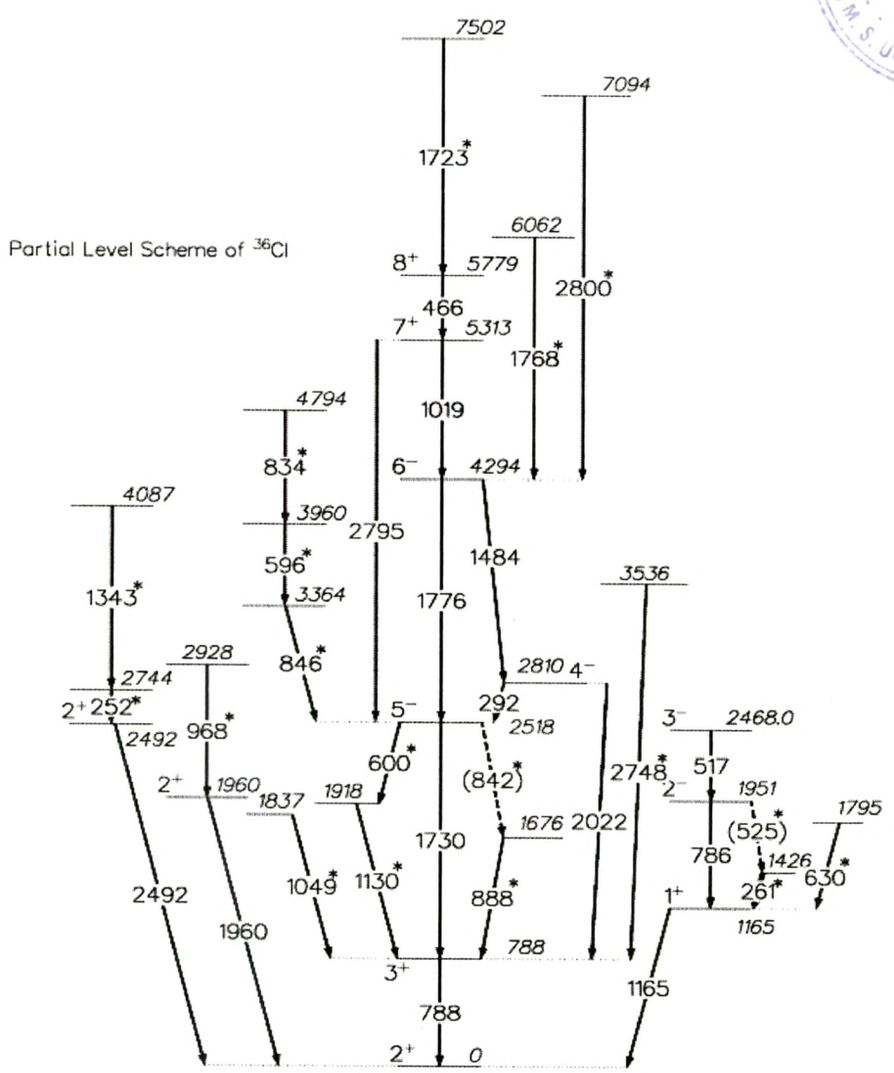

Figure 5.1: Level Structure of ^{36}Cl with the newly found γ-transitions marked by an asterisk.

Fig. 5.2 illustrate representative background subtracted γ spectra with gate on the first three transitions of the yrast band 788+1730+1776-keV transitions. A gate on the newly found transition 2800-keV is displayed in Fig. 5.3. Fig. 5.4 to Fig. 5.6 illustrate the individual spectra of 788- ($3^+ \rightarrow 2^+$), 1730- ($5^- \rightarrow 3^+$) and 1776-keV ($6^- \rightarrow 5^-$). In Fig. 5.2 we can observe the transitions that are in coincidence with the 788+1730+1776-keV transitions. All the transitions were carefully placed into the level scheme [Fig. 5.1.] through coincidence measurements. The newly found γ-transiton 2800-keV which is very

close to the known 2795-keV transition is shown in the index of the figure. Identifying the 2800-keV transition is an example to show the good resolution of the Clover detectors used. Fig. 5.3 shows the comparison of the close-lying γ transitions 2795- and 2800-keV.

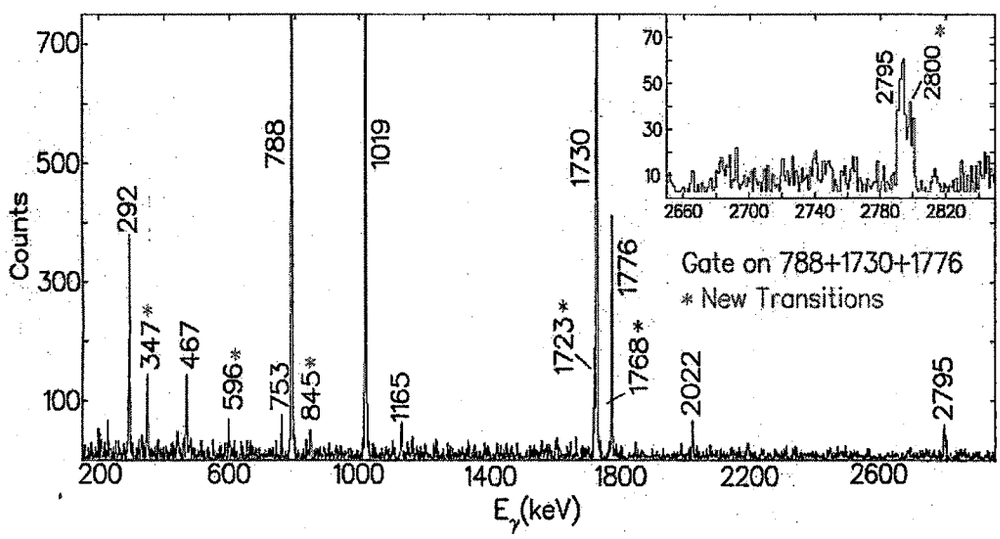

Figure 5.2: Background subtracted gated spectra of 788+1730+176-keV transitions belonging to ^{36}Cl. The newly found transitions are marked with an asterisk.

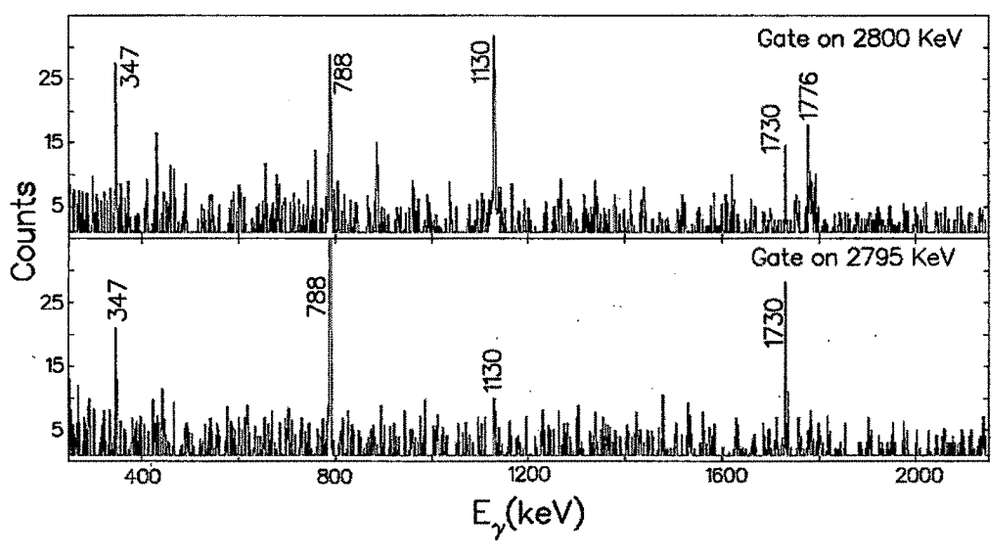

Figure 5.3: Background subtracted gated spectra of 2795- and 2800-keV transitions. The figure presents the validity of the 2800-keV transition, which is placed above the 4294-keV level.

In the top protion of the Fig. 5.3 we can clearly see the 1776-keV but cannot be seen in the gate on 2795-keV (lower portion). This clearly indicates that the 2800-keV is in coincidence with the 1730- and 1776-keV transitions were as the 2795-keV is not in coincidence with the 1776-keV transition. In the same way we could also observe the 1723- and 1768-keV γ-ray transitions. The 1723-keV transiton is found in all the gated spectra and is placed in top of the 466-keV transiton, which is de-exciting from the 5277-keV level.

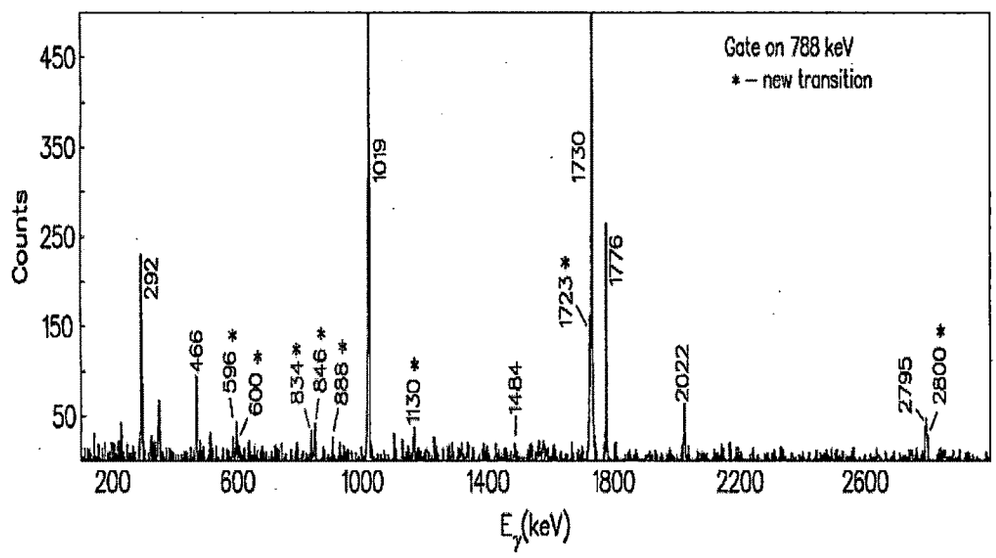

Figure 5.4: The background subtracted gated spectra of 788-keV ($3^+ \rightarrow 2^+$) ground state transition. The newly found ones are marked by an asterisk '*'.

Fig. 5.4 illustrates the background subtracted gated spectra of 788-keV ground state transition. All the known transitions along with the newly ones (marked by 'asterisk') can be seen in the figure. The newly found 600-, 1130-, 888-keV transitons were not seen in the 1730-keV gated spectra [Fig. 5.5]. At the same time they were seen in 1776-keV gated spectra [Fig. 5.6]. As an inference they were placed in anti-coincidence to the 1730-keV transition and in coincidence to 1776-keV transition. The known transtions 292-, 1484-, 2795-keV are not in coincidence as observed in Fig. 5.6. They are placed in anti-coincidence to the 1776-keV transiton. The transitions 596-, 846-, 834-keV were in coincidence with both the 788- and 1730-keV gates, but in anti-coincidence to 1776-keV transition. They were placed on above the 2518-keV level. The

other transitions 1049- and 2748-keV were in coincidence only with the 788-keV ground state transition and they were accordingly placed.

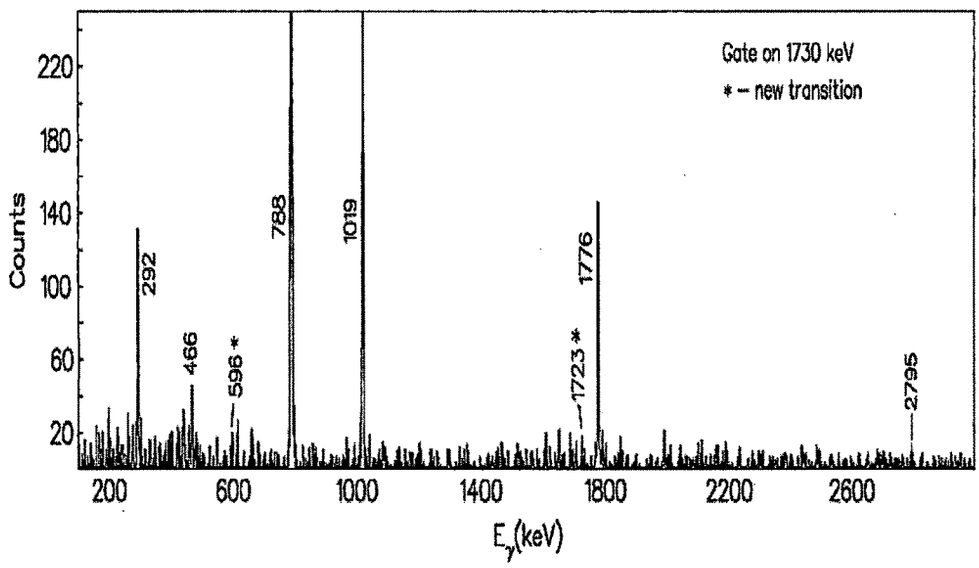

Figure 5.5: The background subtracted gated spectra of 1730-keV ($5^- \rightarrow 3^+$) transition. The newly found ones are marked by an asterisk '*'.

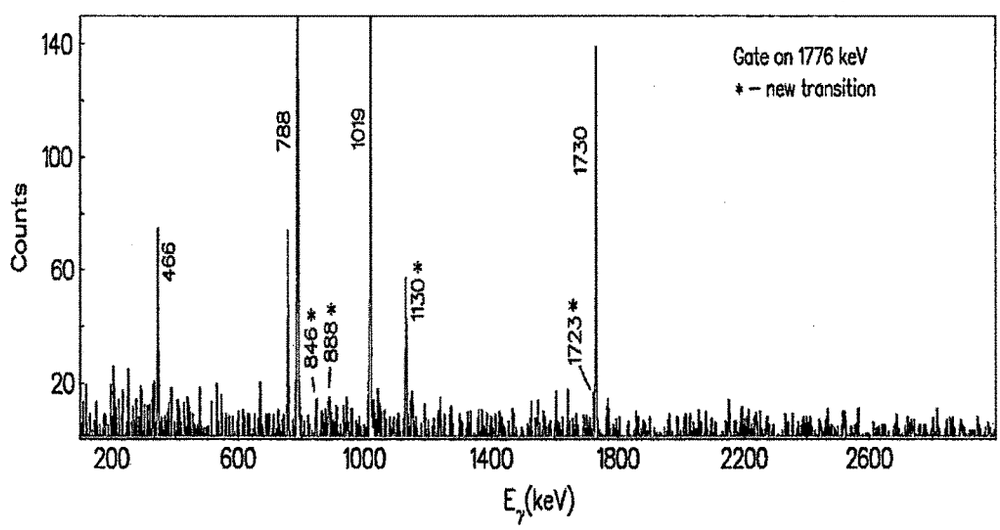

Figure 5.6: The background subtracted gated spectra of 1776-keV ($6^- \rightarrow 5^-$) transition. The newly found ones are marked by an asterisk '*'.

The other non-yrast γ-rays found are through the 1960-, 2492-, 1165-keV gated transitions. Refer to the Fig. 5.7, the γ-rays 786-, 517-, 631-, 261-keV are all in coincidence with 1165-keV ($1^+ \rightarrow 2^+$) ground state transition. The 786-keV transition is not in coincidence with 261- and 631-keV γ-rays. Hence they are placed accordingly.

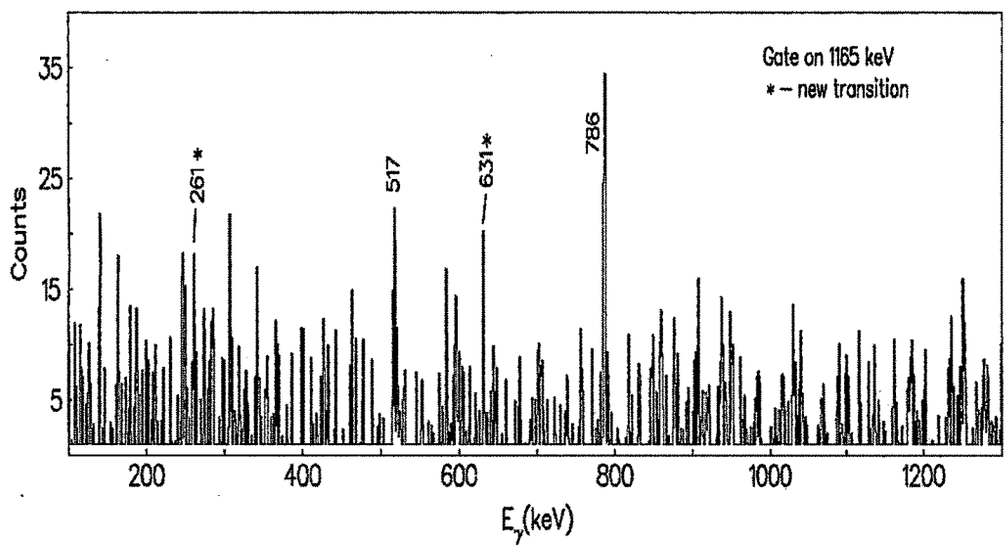

Figure 5.7: The background subtracted gated spectra of 1165-keV ($1^+ \rightarrow 2^+$) transition. The newly found ones are marked by an asterisk '*'.

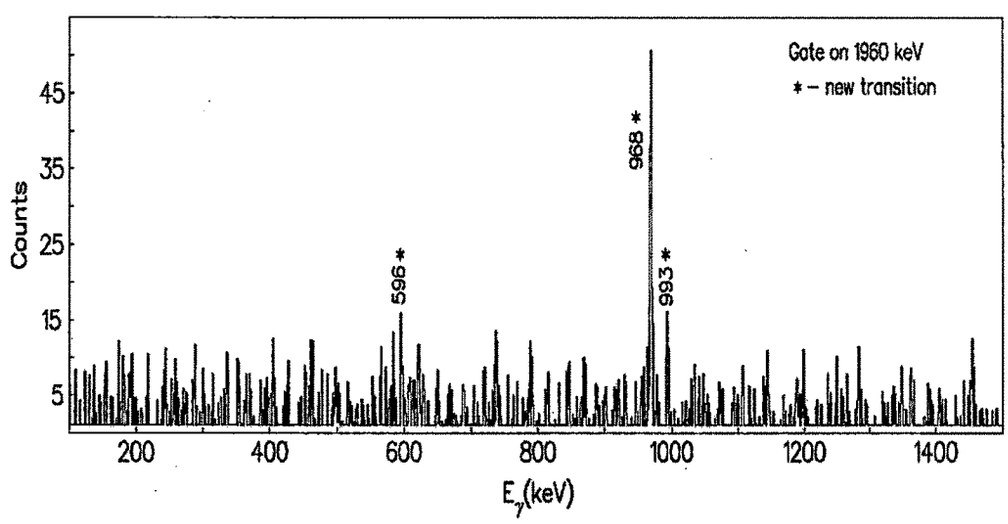

Figure 5.8: The background subtracted gated spectra of 1960-keV ($2^+ \rightarrow 2^+$) transition. The newly found ones are marked by an asterisk '*'.

In the other ground state transition 1960-keV ($2^+ \rightarrow 2^+$) (Fig. 5.8) we have observed 968-keV which is in coincidence. And also 993-keV which couldn't be placed in the present level scheme due to the complex nature of the level structure of ^{36}Cl. We have also observed two new γ-rays in the gated ground state spectra of 2492-keV (Fig. 5.9). The 252- and 1343-keV transitions are in coincidence with the 2492-keV and vice-versa. The level and transition energies, γ-ray intensities, and multipolarity assignments are summarized in table 5.1.

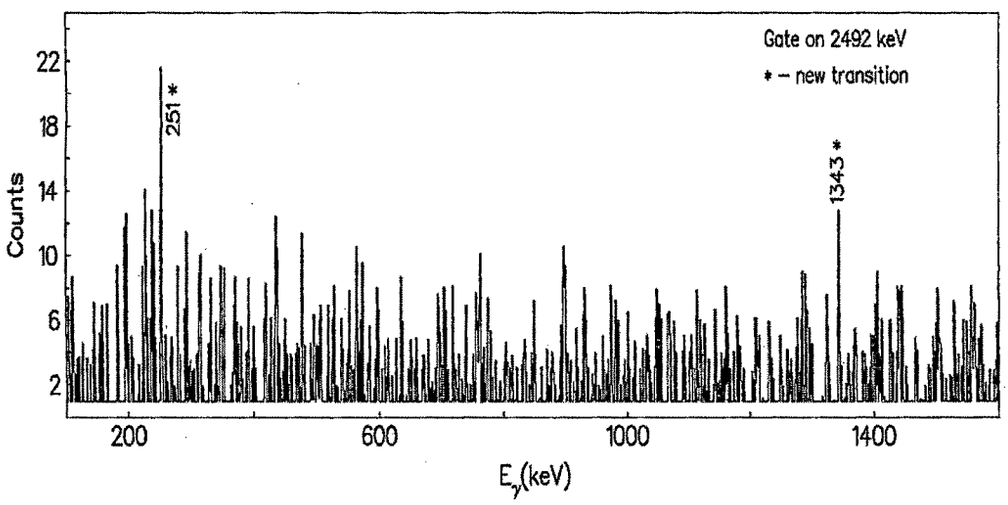

Figure 5.9: The background subtracted gated spectra of 2492-keV ($2^+ \rightarrow 2^+$) transition. The newly found ones are marked by an asterisk '*'.

Table 5.1: γ transition energy (E_γ) in keV, excitation energy (E_x) in keV, relative γ-ray intensities (I_γ), Multipolarity, initial and final spins for the transitions belonging to ^{36}Cl.

Gamma Energy (Eγ) keV	**Level Energy (Ex) keV**	**Intensity (Iγ)**	**Multipolarity**	$J_i^\pi \rightarrow J_f^\pi$
261.0	1426.0			
292.0	2810.0	15.10 (1.06)	M1	$4^- \rightarrow 5^-$
466.0	5779.0	5.57 (0.28)	M1	$8^+ \rightarrow 7^+$
517.0	2468.0		M1	$3^- \rightarrow 2^-$
525.0	1952.0			
596.0	3960.0	2.62 (0.08)		

600.0	2518.0	1.24 (0.05)		
630.0	1795.0			
786.0	1951.0		E1	$2^- \rightarrow 1^+$
788.0	788.0	100.0	M1	$3^+ \rightarrow 2^+$
834.0	4794.0	1.67 (0.03)		
842.0	2518.0			
846.0	3364.0	3.94 (0.10)		
888.0	1676.0			
968.0	2928.0			
1019.0	5313.0	31.38 (2.82)		
1049.0	1837.0			
1130.0	1918.0	1.31 (0.026)		
1165.0	1165.0		M1	$1^+ \rightarrow 2^+$
1343.0	4087.0			
1484.0	4294.0	0.99 (0.02)	E2	$6^- \rightarrow 4^-$
1723.0	7502.0	12.32 (0.86)		
1730.0	2518.0	92.77 (4.6)	M2	$5^- \rightarrow 3^+$
1768.0	6062.0	0.76 (0.02)		
1776.0	4294.0	15.21 (1.8)	M1	$6^- \rightarrow 5^-$
1960.0	1960.0		E2	$2^+ \rightarrow 2^+$
2022.0	2810.0	4.43 (0.57)	E1	$4^- \rightarrow 3^+$
2492.0	2492.0		E2	$2^+ \rightarrow 2^+$
2748.0	3536.0	1.06 (0.03)		
2795.0	5313.0	4.16 (0.33)	M2	$7^+ \rightarrow 5^-$
2800.0	7094.0	2.32 (0.21)		

[a] All the gating transitions are pure dipole transitions; [b] The quoted errors on intensities include errors due to background subtraction, fitting, and efficiency correction.

5.5.2. Level Structure of ^{54}Mn

In addition to the earlier known transitions, nine new γ-transitions belonging to ^{54}Mn have been placed in the decay scheme based on the coincidence, intensity arguments and the presence of cross-over transitions (Fig. 5.10). A representative γ-γ prompt coincidence spectrum with a gate on sum of a few low-lying transitions is shown in Fig. 5.11. Fig. 5.12 illustrates the spectrum with a gate on one of the newly observed γ-transitions where all other transitions belonging to the sequence are clearly seen. The contamination from neighbouring nuclei is identified and marked accordingly in both the spectra. The specific contaminants observed in the spectra which belong to the neighbouring nuclei, namely ^{48}V, ^{58}Co, ^{64}Cu, ^{65}Zn are shown in Fig. 5.11 (gate on sum of 156+212+705-keV transitions) and ^{56}Fe, ^{64}Zn, ^{64}Cu, ^{68}Ge in Fig. 5.11 (gate on 847-keV transition). The contamination observed in the spectra are listed in table 5.2. The imbalance in intensities in the coincidence spectra could be attributed to the aforementioned contamination.

The angle dependent E_γ - E_γ matrices were used to obtain the intensity anisotropy for the observed γ-transitions; which were then used to assign qualitatively the spin of the level de-exciting by the particular transition. The γ-γ matrix was constructed with one axis corresponding to the data recorded in the 90° detectors and the other axis contained the coincidence data from the 40° detectors. R_{DCO} is then defined as:

$$R_{DCO} = \frac{I_{\gamma_1} \text{ at } 90°, \text{ gated with } \gamma_2 \text{ at } 40°}{I_{\gamma_2} \text{ at } 40°, \text{ gated with } \gamma_2 \text{ at } 90°} \qquad (5.1)$$

Table 5.2: List of contaminants observed in the given spectra from various neighbouring nuclei.

E_γ (keV)	Contamination
333	^{58}Co
608	^{48}V
202, 459, 480, 785, 1019	^{64}Cu
511	^{65}Zn
266, 367, 859, 945, 970, 991, 1039	^{56}Fe
191,202,612,695	^{68}Ge
342, 511	^{64}Zn
846	^{39}Ca

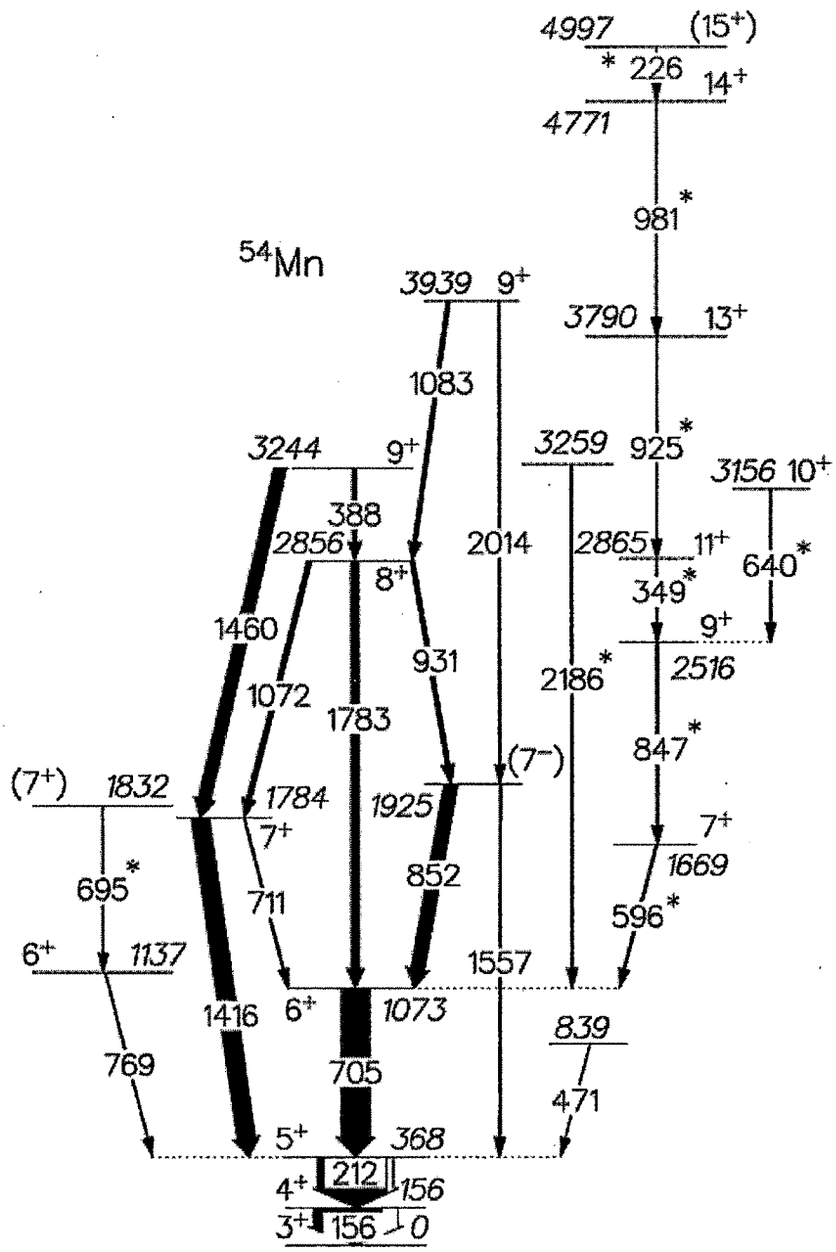

Figure 5.10: Level Scheme of ^{54}Mn for the levels populated in $^{20}Ne + ^{51}V$ reaction at 145 MeV. Newly observed transitions are marked with an asterisk. The width of the arrows is approximately proportional to the observed intensities.

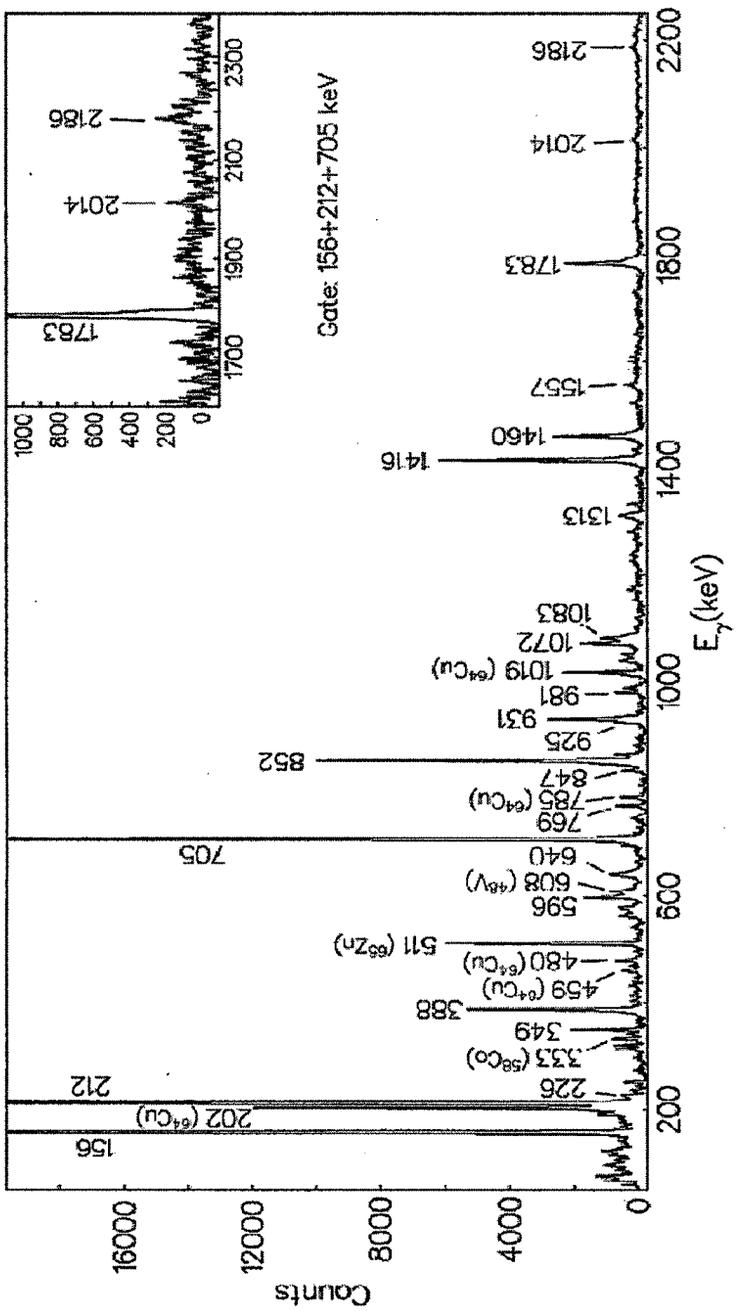

Figure 5.11: γ-γ Coincidence spectrum for ^{54}Mn with simultaneous gates on the 156-($4^+ \rightarrow 3^+$), the 212- ($5^+ \rightarrow 4^+$) and the 705-keV ($6^+ \rightarrow 5^+$) transitions. The energies are marked within ± 1 keV. The contaminant gamma ray transitions are indicated with their respective origin of nuclei.

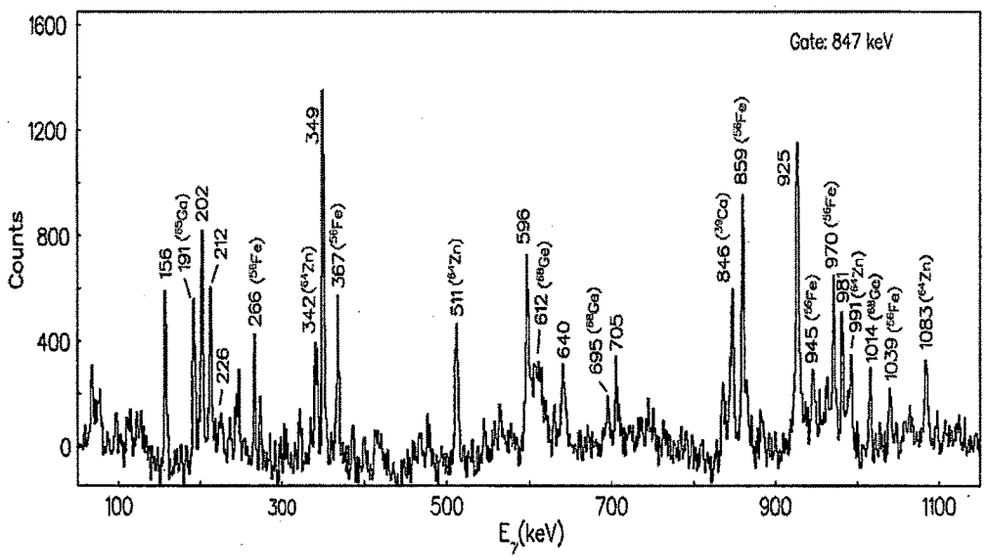

Figure 5.12: γ-γ Coincidence spectrum for ^{54}Mn with gate on the 847-keV ($9^+ \rightarrow 7^+$) newly found transition. The contaminant gamma ray transitions are indicated with their respective origin of nuclei.

Assuming the commonly encountered situation of stretched transitions, the value of R_{DCO} for those γ-rays having the same multipolarity as the gated γ-ray would be ~ 1, while the value differs by a factor of ~ 2 if the multi-polarities of the gamma rays were different. The resultant values of R_{DCO} for some of the observed transitions are illustrated in Fig. 5.13. The present statistics allowed us to obtain only qualitative information regarding the multipolarities of the transitions. Quantitative estimates such as mixing ratios could not be obtained due to the limited statistics in the angle dependent data analysis (Refer to Chapter. 4 for detailed information regarding the DCO and Polarization measurements).

The use of Clover detectors facilitates polarization measurements. In a Clover each of the individual crystal acts as a scatterer, while the two adjacent crystals as the absorbers. The anisotropy between the number of Compton scattered γ-rays in the reaction plane $N_{||}$, and perpendicular to it, $N_{\perp}$, is indicative of the electromagnetic nature of the transition. Even though the statistics in the present experiment permitted only qualitative polarization estimates, these in conjunction with the coincidence angular correlation measurements were crucial for the assignment of the spins and parities of the observed transitions.

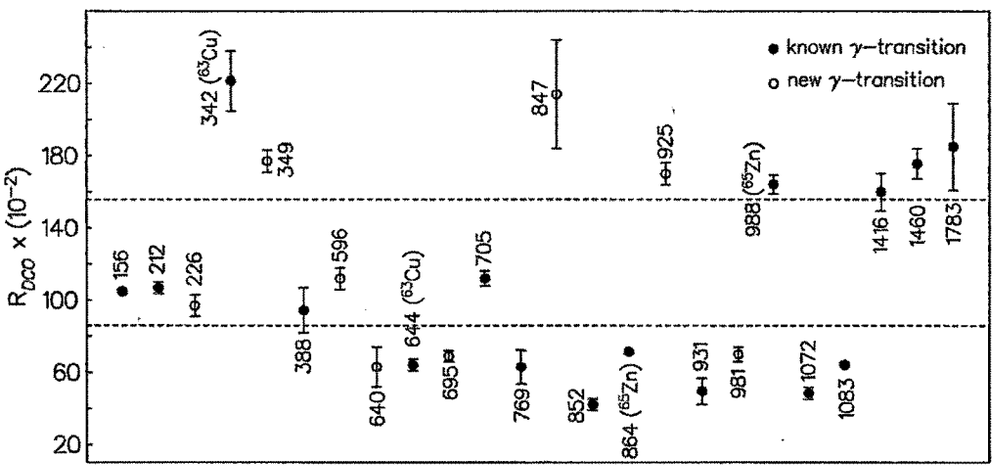

Figure 5.13: Gamma-ray asymmetry R_{DCO} plotted as a function of the γ-ray energy. The lines have been drawn to guide the eye correspond to the average values of ~ 0.88 for a dipole transition and ~ 1.6 for quadruple transition when gated on a pure dipole transition. The quoted errors include the errors due to background subtraction, fitting and efficiency correction.

A polarization matrix was constructed where the energy recorded in a detector was placed on one axis, while the other axis correspond to the energy scattered in a perpendicular or a parallel segment of the Clover with respect to the beam axis [44, 45]. From the projected spectra, the number of perpendicular ($N_{\perp}$) and parallel ($N_{\parallel}$) scatters for a given γ-ray could be obtained. From these spectra the asymmetry of the Compton scattered polarized photons was obtained using the relation:

$$\Delta_{IPDCO} = \frac{a(E_\gamma)N_\perp - N_\parallel}{a(E_\gamma)N_\perp + N_\parallel} \tag{5.2}$$

The correction parameter 'a' is the term due to the asymmetry of the present experimental configuration. It is defined as:

$$a = \frac{N_\parallel(unpolarized)}{N_\perp(unpolarized)} \tag{5.3}$$

The correction term here is determined from the unpolarized ^{152}Eu source. The variation of 'a' with E_γ, fitted with the expression $a(E_\gamma) = a_0 + a_1(E_\gamma)$ results in a_0 = 0.996 and a_1= -1.53 * 10^{-6} where E_γ is in keV. Fig. 5.14 illustrates the asymmetry

parameter '*a*' for the current experimental setup. Asymmetry parameter '*a*' is calculated from the efficiency data obtained using the ^{152}Eu radioactive source.

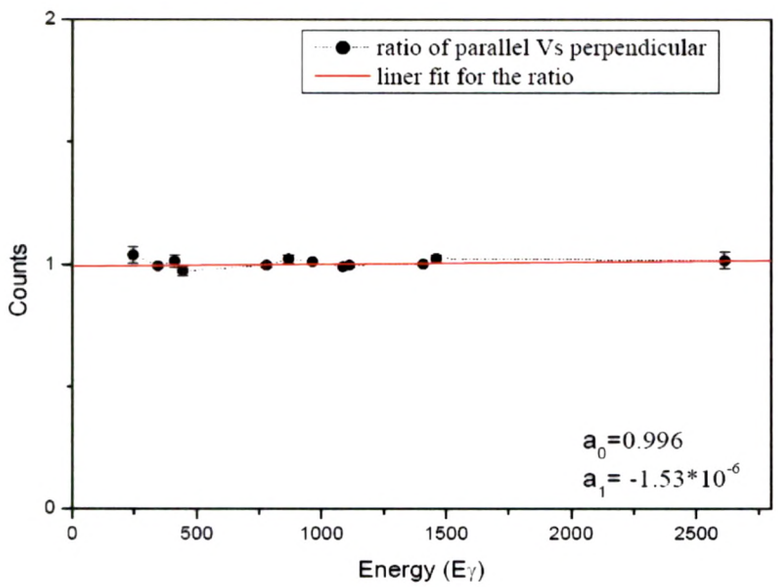

Figure 5.14: Graph showing the asymmetry parameter '*a*', obtained from the radioactive decay data of ^{152}Eu.

Recently several authors have demonstrated the feasibility of extending this procedure to nuclei populated following non-equilibrated reactions as the present nucleus ^{54}Mn is populated predominantly through incomplete fusion reaction mechanism [44]. In the figure below (Fig. 5.15.) we plot the Δ_{IPDCO} for some of the strong transitions populated in the neighbouring nuclei, whose multipolarities have been established.

A pure electric transition due to its preferential scattering in the perpendicular direction with respect to the beam axis, results in a positive value for $\Delta_{IPDCO.}$ While a pure magnetic transition results in a negative value for Δ_{IPDCO} due to its preferential scattering along the parallel direction. A near-zero value for Δ_{IPDCO} is indicative of an admixture. Fig. 5.16 illustrates the value of asymmetry parameter for some of the observed transitions in ^{54}Mn. For comparison the value of DCO and IPDCO for a few known transitions (whose multi-polarity has been firmly established) from neighbouring nuclei are also shown in the figures. The analysis of the angle dependant data and the polarization data sets is performed from relatively clean gates which at times have resulted in poor statistics.

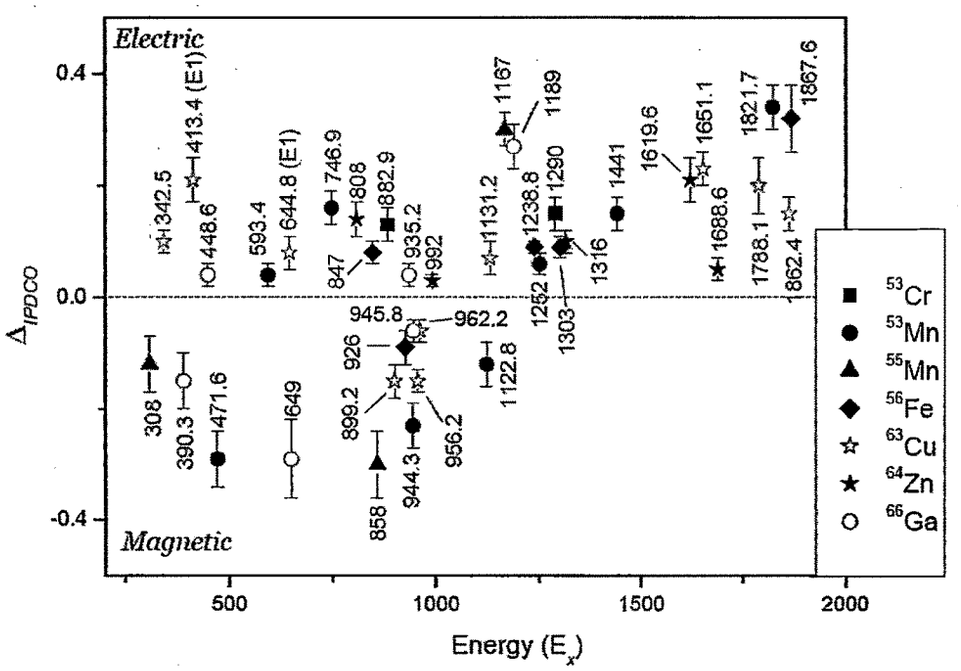

Figure 5.15: Representative experimental γ-ray asymmetry parameter, from polarization measurements plotted for γ-transitions in the populated nearby nuclei.

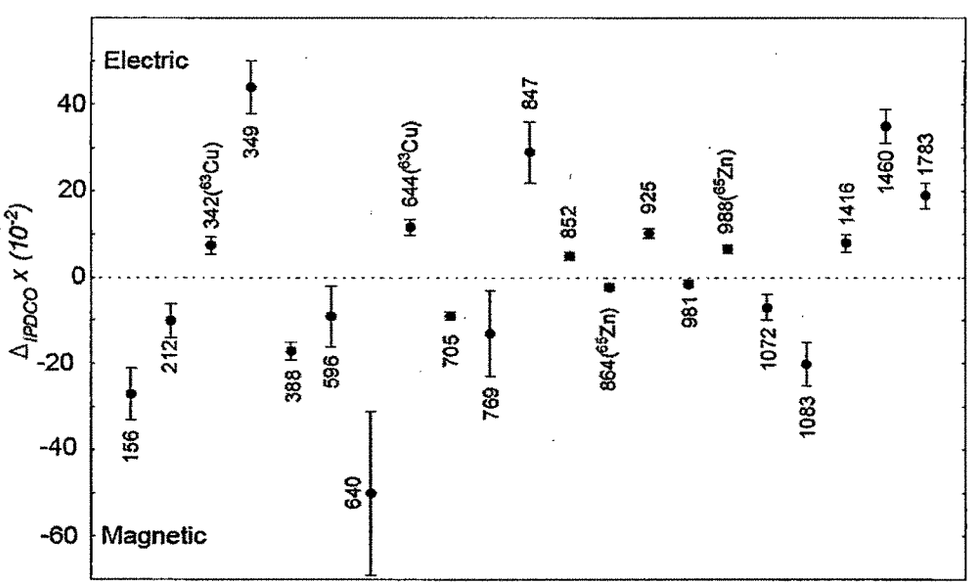

Figure 5.16: Representative experimental γ-ray asymmetry parameter, from polarization measurements plotted for γ-transitions in ^{54}Mn. A positive value corresponds to an electric transition and a magnetic transition results in a negative value. The quoted errors consists error due to background subtraction and fitting.

Difference of parallel and perpendicular background subtracted gated spectra of simultaneous gates on 156/212/705- and 156-keV transitions are presented in Fig. 5.17, 5.18. In the figures the γ transitions towards the positive side present the '*electric*' nature and transitions on the negative side presents the '*magnetic*' nature of those transitions respectively.

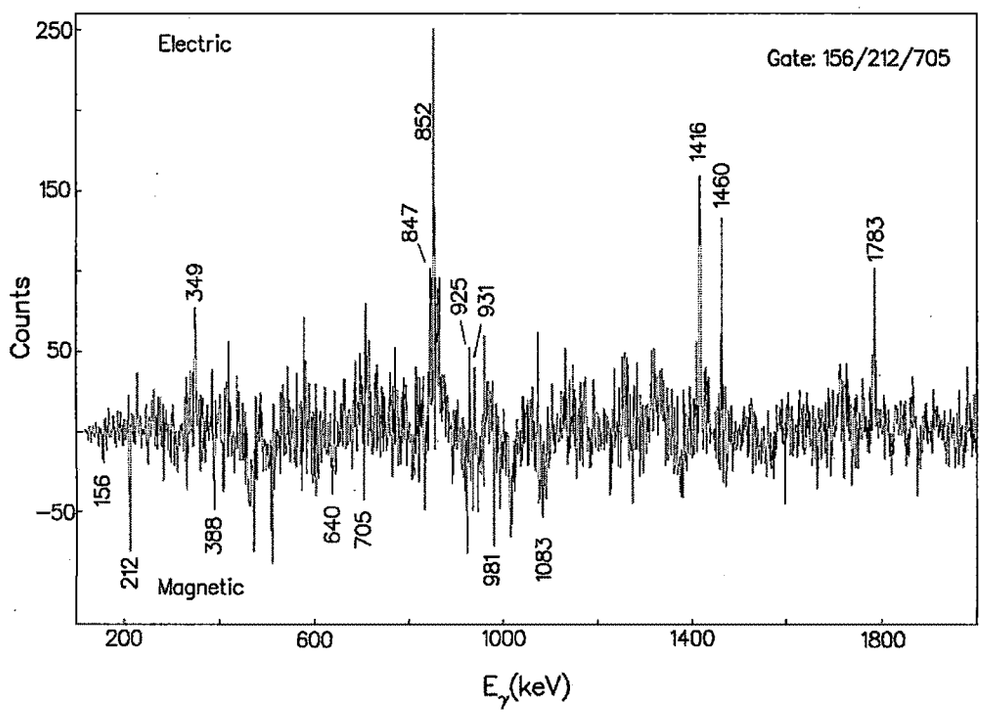

Figure 5.17: Difference of parallel and perpendicular polarization spectra of simultaneous gates on 156/212/705-keV belonging to ^{54}Mn.

The level scheme of ^{54}Mn has been established upto $E_x \sim 5$ MeV in excitation energy and a tentative spin of $J \sim 15\hbar$ (Fig. 5.10). In addition to the transitions reported by Toulemonde *et al.,* [35], about nine new transitions have been identified in the present work. These transitions are indicated by an asterisk in the level scheme. The quality of the data set is clear from a representative background-subtracted gated spectrum shown in Fig. 5.19. A few other gated spectra of γ-rays belonging to ^{54}Mn associated with the yrast band are shown in Fig. 5.20, 5.21.

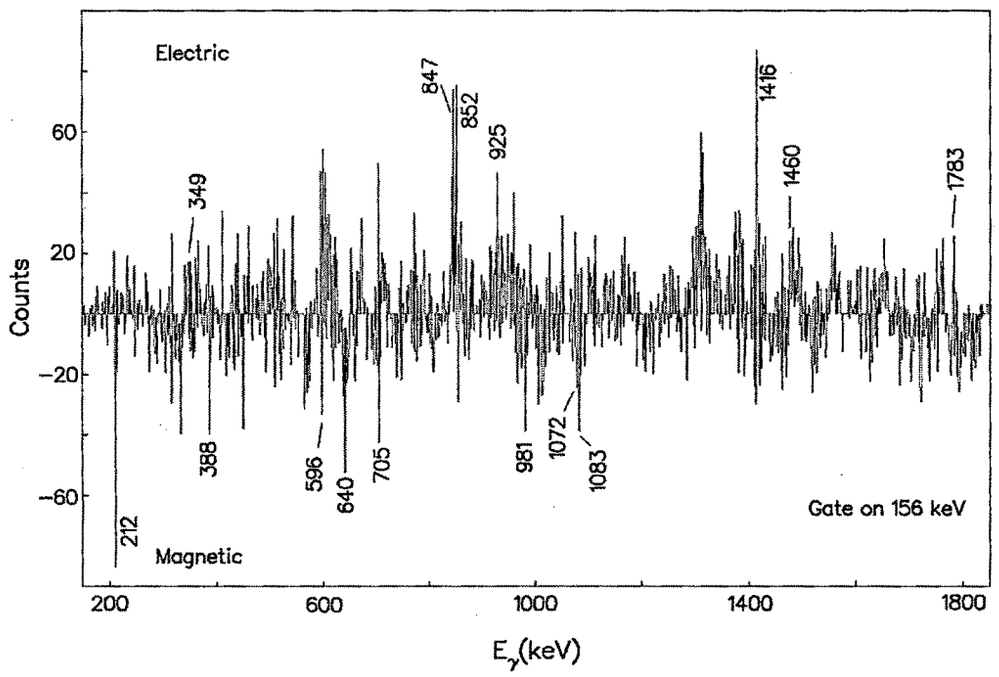

Figure 5.18: Difference of parallel and perpendicular polarization spectra of 156-keV gate belonging to ^{54}Mn.

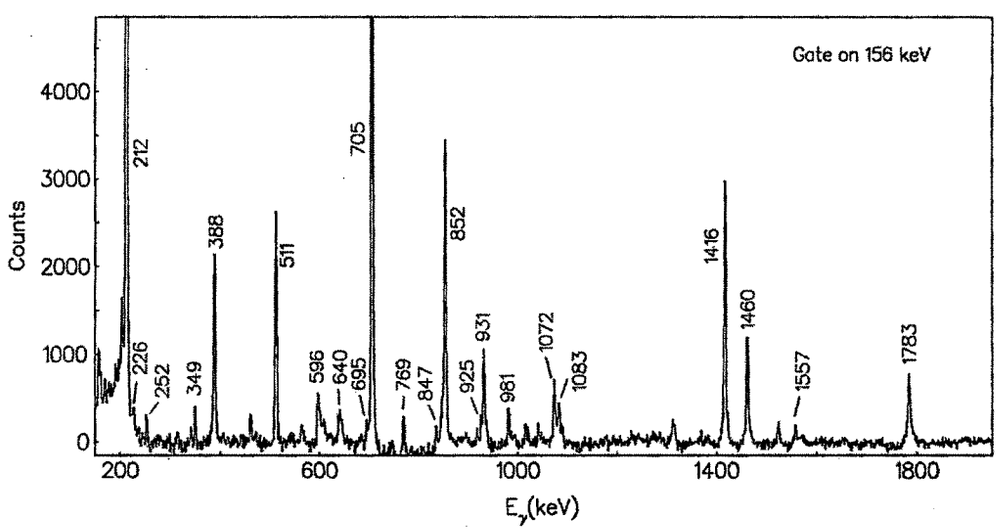

Figure 5.19: Representative γ-γ coincidence background-subtracted gated spectrum of 156-keV ($4^+ \rightarrow 3^+$) transition.

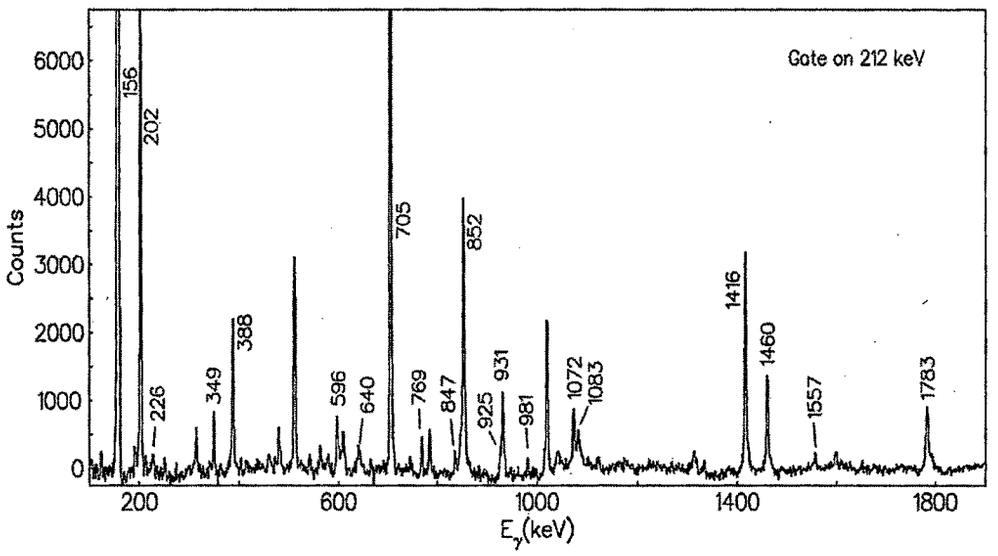

Figure 5.20: Representative γ-γ coincidence background-subtracted gated spectrum of 212-keV ($5^+ \rightarrow 4^+$) transition.

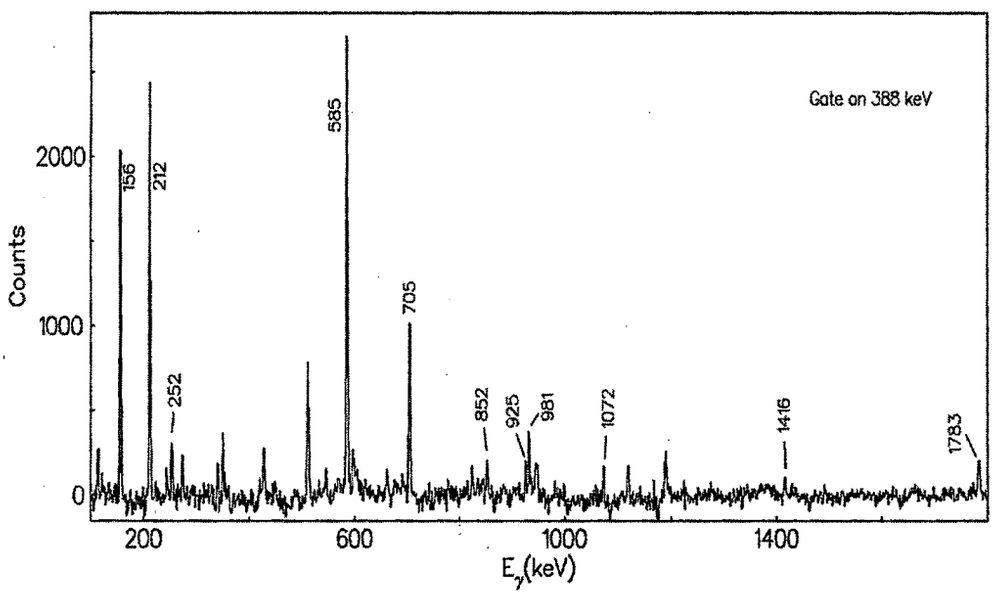

Figure 5.21: Representative γ-γ coincidence background-subtracted gated spectrum of 388-keV ($9^+ \rightarrow 8^+$) transition.

In the present work, almost all transitions observed by Poletti *et al.* [32], Toulemonde *et al.* [35], as belonging to ^{54}Mn were identified. Radford and Poletti [34],

have observed a series of three bands using (α, n) reactions. In the present study the high-spin yrast states that are normally expected to be excited in the heavy-ion reactions have been observed. The 408-keV transition reported by Poletti *et al.* [32], and the 368-keV yrast transition reported by Radford and Poletti [34] are not found in the present study due to the lack of coincidence data for these γ-rays. The 252-keV transition [32] although observed could not be placed into the level scheme due to its low statistics in the coincidence spectra.

The major discrepancy with the level scheme reported by Poletti *et al.* [36], is regarding the placement of the 388-keV transition. The present coincidence data indicates that this transition is in coincidence with the 1783-keV transition, and is not in parallel with the 1783-keV transition as reported earlier [32]. Hence this transition has accordingly been placed in the level scheme. The same has been observed by Toulemonde *et al.* [35], but it was given a tentative spin of 9. The electromagnetic nature for this transition could be uniquely assigned from our multipolarity calculations. Our present measurement indicate that for this transition we obtain a DCO value of 0.91 (0.12) when gated on a dipole transition and Δ_{IPDCO} = 0.05 (0.01). This clearly indicates that the transition 388-keV is a magnetic dipole (M1). In the present work, the spin of the level 3244-keV was confirmed as 9^+. The present assignment is in accordance with the placement by Toulemonde *et al.* [35]. Further we have been able to assign the spin-parity for the earlier reported levels [32].

Toulemonde *et al.* [35], have reported linear polarization measurements for levels in ^{54}Mn populated following the ^{52}Cr(α, pnr) reaction at 33 MeV [8MeV/A]. The present results are in agreement with earlier polarization measurements. However, the associated errors in the present measurements are considerably lower than the earlier values. This comparison demonstrates the feasibility of undertaking the polarization measurements and could provide a figure-of-merit for the present results. A qualitative comparison of the present results and those reported by Toulemonde *et al.*, is presented in the table 5.3.

The polarization measurements by Toulemonde *et al.* [35], for the 852- and 931-keV transitions had considerable errors, making the spin parity assignments for the level at 1925-keV rather ambiguous. The polarization measurements of Toulemonde *et al.* [35], had a large error for the measured linear polarization for the 852-keV transition (-0.03 (0.05)). Hence, the electromagnetic nature for this level could not be uniquely assigned. Our present measurement indicate that for this transition we obtain a value of Δ_{IPDCO} =

0.05 (0.01). The 156-keV and 852-keV γ-rays also belong to ^{64}Zn. Hence Δ_{IPDCO} for the 852-keV transition was obtained from other clean gates such as 212- and 705-keV, to name a few, which yielded a positive value for the Δ_{IPDCO}.

Thus a positive value is indicative of an electric nature for the 852-keV transition. Further, our angular distribution is consistent with the earlier reported ΔJ=1 nature for this transition. Hence, these measurements are indicative for the $J^{\pi} = 7^{-}$ assignment for the level at 1925-keV which de-excites predominantly via the 852-keV transition. However, this would have to be corroborated by the polarization measurements for the other transitions feeding and de-exciting from this level. The polarization measurement for the 931-keV transition which feeds this level is crucial to confirm the present assignment. Unfortunately the 931-keV transition is in coincidence with the 156-, 212- and 705-keV transitions in other neighbouring nuclei, and the transition is predominantly magnetic in nature in these nuclei.

Table 5.3: Table presents a qualitative comparison of present polarization (Δ_{IPDCO}) values to that of the ones reported by Toulemonde *et al.* [39].

E_γ	**Toulemonde *et al.*,**	**Present**
212	-0.33(0.2)	-0.036(0.01)
705	-0.29(0.3)	-0.013(0.01)
1416	0.55(0.9)	0.10(0.01)
1783	0.63(0.16)	0.20(0.03)
1072	-0.03(0.18)	-0.07(0.03)
931	0.01(0.08)	-
387	-0.51(0.16)	-0.17(0.02)
1081	-0.13(0.18)	-0.20(0.02)
852	-0.03(0.05)	0.05(0.01)

The earlier polarization measurements for the 931-keV transition feeding the 1925-keV level was also inconclusive (0.01 (0.08)) due to the large errors. The polarization measurements for the 931-keV transition could not be done with sufficient accuracy from relatively clean gates, in the present experiment, as the 931-keV transition is in coincidence with the 156-, 212- and 705-keV transitions in other neighbouring nuclei. We could not obtain the Δ_{IPDCO} value for the transition with sufficient accuracy

from relatively clean gates and hence the Δ_{IPDCO} value for this transition has not been mentioned in our measurements.

Our measurements for the other gamma rays (1557-keV and 2014-keV) connected to the 1925-keV level could not unambiguously assign its electromagnetic nature due to large errors and poor statistics. The 1557-keV transition involves a $\Delta J = 2$ change in angular momentum which is in agreement with the previous measurements [36, 38, 39]. Hence the possible electromagnetic nature for this transition could be either an E2 or M2. Assuming E2 and M2 the single particle estimate, the lifetime for the 1557-keV transitions are in 10^{-12} and 10^{-10} sec range respectively. From lifetime considerations both these are possible and are within our prompt resolving time. The analysis of the polarization data for this transition qualitatively indicated a negative value -0.14 (0.1) for the asymmetry parameter. However, the statistics did not permit us to obtain a quantitative value along with the associated errors for this transition. Hence, the value has not been included in the figure as well as the table. However, the indication of a magnetic nature to the 1557-keV transition corroborates the present $J^{\pi} = 7^{-}$ assignment for the 1925-keV level. A similar situation prevails for the 2014-keV transition where the IPDCO value for this transition is -0.09 (0.06). This again is qualitative due to large associated errors.

Further, the polarization asymmetry for the 2186-keV transition qualitatively indicated that this is a mixed transition. These observations did not permit us to make unambiguous assignment for the parity of the 1925-keV level. However, these results warrant further detailed investigations on this level which could have an unnatural parity or the 852-keV transition could have substantial admixture. Hence, the level at 1925-keV is tentatively assigned a negative parity. One does not expect a negative parity level at such low excitation energy in this odd-odd nucleus, and in fact such levels have not been observed in the neighbouring odd-odd nuclei [33, 46 - 48]. Apart from these changes we have observed several new transitions belonging to the nucleus ^{54}Mn for the first time.

The occurrence of cross-over transitions such as the 1416-keV (E2), 1460 keV (E2) corroborates the placement for a few of the newly observed transitions. The newly observed transitions are 695(M1), 2186(E2), 596(M1), 847(E2), 349(E2), 925(E2), 981(M1), 226(M1), 640(M1). A sequence comprising of a majority of $\Delta J = 2$ electric transitions above the 1073-keV level, has been observed for the first time. The members of the band are 596(M1), 847(E2), 349(E2), 925(E2), 981(M1), 226(M1), 640(M1). The

R_{DCO} and Δ_{IPDCO} values 640-keV transition are indicative of a magnetic nature for this transition. The 226-keV transition has been tentatively assigned as a M1 transition based on the observed R_{DCO} value.

The 769-keV transition reported in Ref. [32] has been assigned as M1 based on the R_{DCO} and Δ_{IPDCO} values viz. 0.61 (0.09) and -0.13 (0.1) respectively. The 695-keV transition placed above this transition is tentatively assigned a M1 nature based on the observed R_{DCO} = 0.69 (0.03) value. We could not assign a parity for this transitions due to poor statistics with the gated γ-γ coincidence polarization spectra. The level and transition energies, γ-ray intensities, DCO and IPDCO ratios, and deduced spin-parity assignments are summarized in table 5.4. The intensities of the all the γ-rays reported were obtained from the spectrum gated by the 212-keV transition.

Table 5.4: γ transition energy (E_γ) in keV, excitation energy (E_x) in keV, DCO ratios (R_{DCO}), IPDCO ratios (Δ_{IPDCO}), relative γ-ray intensities (I_γ), Multipolarity, initial and final spins for the transitions belonging to ^{54}Mn.

E_γ	E_x	R_{DCO} [a]	Δ_{IPDCO}	I_γ [b] (%)	*MULTIPO -LARITY*	$J_i^\pi \rightarrow J_f^\pi$
156.21	156	1.01 (0.01)	-0.27 (0.06)	100	M1	$4^+ \rightarrow 3^+$
211.96	368	1.03 (0.03)	-0.10 (0.04)	100	M1	$5^+ \rightarrow 4^+$
226.43	4997	0.97 (0.06)	-	0.45 (4.8)	(M1)	$15^{(+)} \rightarrow 14^+$
348.79	2865	1.77 (0.06)	0.44 (0.06)	1.54 (2.7)	E2	$11^+ \rightarrow 9^+$
387.70	3244	0.91 (0.12)	-0.17 (0.02)	5.81 (1.5)	M1	$9^+ \rightarrow 8^+$
471.00	839	-	-	0.56 (3.7)	-	-
596.30	1669	1.12 (0.06)	-0.09 (0.07)	2.69 (2.3)	M1	$7^+ \rightarrow 6^+$
639.78	3156	0.63 (0.11)	-0.50 (0.19)	1.57 (3.8)	M1	$10^+ \rightarrow 9^+$
694.98	1832	0.69 (0.03)	-	1.40 (2.0)	(M1)	$7^{(+)} \rightarrow 6^+$
704.87	1073	1.08 (0.04)	-0.09 (0.01)	41.04 (0.4)	M1	$6^+ \rightarrow 5^+$

711.00	1784	-	-	2.13 (2.5)	M1	$7^+ \rightarrow 6^+$
768.94	1137	0.61 (0.09)	-0.13 (0.1)	1.31 (2.8)	M1	$6^+ \rightarrow 5^+$
847.39	2516	2.14 (0.30)	0.29 (0.07)	2.69 (2.1)	E2	$9^+ \rightarrow 7^+$
852.35	1925	0.41 (0.03)	0.05 (0.01)	19.75 (0.8)	(E1)	$7^{(-)} \rightarrow 6^+$
925.43	4771	1.70 (0.06)	0.102 (0.01)	1.31 (4.0)	E2	$13^+ \rightarrow 11^+$
931.04	2856	0.48 (0.07)	-	5.52 (1.5)	M1/E1	$8^+ \rightarrow 7^{(-)}$
980.59	3846	0.70 (0.04)	-0.15 (0.09)	1.88 (2.4)	M1	$14^+ \rightarrow 13^+$
1072.37	2856	0.47 (0.03)	-0.07 (0.03)	6.84 (1.4)	M1	$8^+ \rightarrow 7^+$
1082.72	3939	0.62 (0.01)	-0.20 (0.05)	5.11 (1.6)	M1	$9^+ \rightarrow 8^+$
1415.81	1784	1.54 (0.1)	0.08 (0.02)	26.21 (0.7)	E2	$7^+ \rightarrow 5^+$
1460.40	3244	1.69 (0.08)	0.35 (0.04)	18.12 (1.1)	E2	$9^+ \rightarrow 7^+$
1557.20	1925	1.51 (0.34)	-	1.82 (2.9)	(M2)	$7^{(-)} \rightarrow 5^+$
1783.40	2856	1.78 (0.23)	0.19 (0.03)	11.89 (1.6)	E2	$8^+ \rightarrow 6^+$
2014.20	3939	-	-	0.85 (3.9)	(M2)	$9^+ \rightarrow 7^{(-)}$
2185.80	3259	-	-	1.53 (2.7)	-	-

[(a)] All the gating transitions are pure dipole transitions; [(b)] The quoted errors on intensities include errors due to background subtraction, fitting, and efficiency correction.

5.6. Shell Model Calculations

With the increasing success with which the nuclear shell model is being applied to light, medium mass nuclei, it becomes reasonable to hope that a nucleus such as ^{36}Cl, odd-odd but only four nucleons removed from the doubly magic ^{40}Ca, will be amenable to theoretical description within the frame work of this model [9, 49]. The low lying negative parity states of ^{36}Cl should therefore be reasonably well described by the shell-model calculations allowing excitation of particles into $1f_{7/2}$, $2p_{3/2}$ and $2p_{1/2}$ orbitals.

Hoken *et al.*, [48] have carried out the calculations which allowed excitations into the $1f_{7/2}$ and $2p_{3/2}$ orbitals. To interpret the observed level structure of ^{36}Cl, detailed shell-model calculations have also been performed by us using the *fp* Hamiltonian with ^{40}Ca core, available with the code OXBASH [50]. The calculated energy Eigen values are compared with the experimental results in Fig. 5.22.

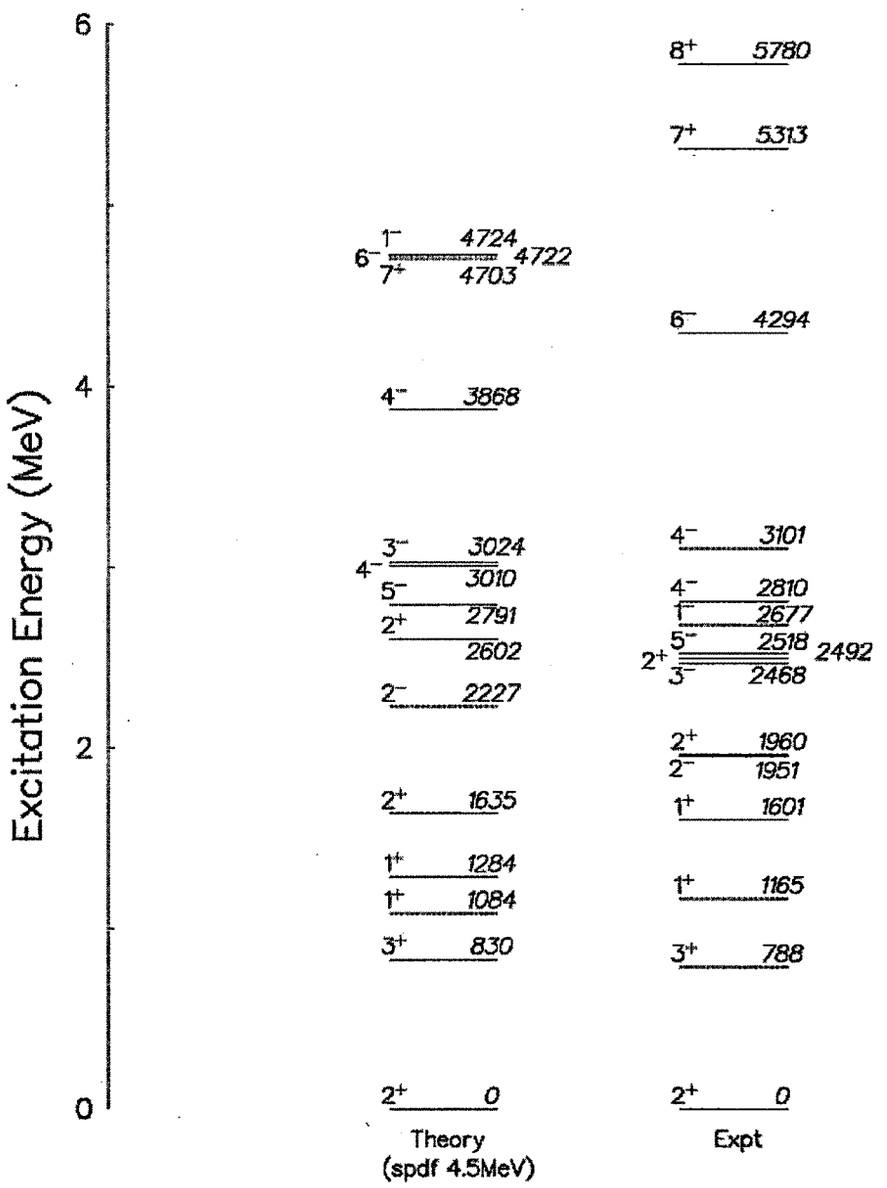

Figure 5.22: Comparison of the experimental levels of ^{36}Cl with the present predictions of the shell model calculations.

To interpret the observed level structure of ^{54}Mn, we have primarily based our discussions on the existing calculations by Johnstone and Benson [39], since our shell model calculations are similar to these calculations. Johnstone and Benson [39] have reported their detailed shell model calculations for ^{54}Mn, wherein they were able to produce the energy level spectrum after incorporating a wide range of configurations. These results are compared with the present level scheme in Fig. 5.10. The comparison is limited to moderate spins and energy [$J^{\pi} = 9^{+}$ and $E_x \sim 3$ MeV]. As seen from the figure the agreement is reasonable. The 6^{+} level at 1073-keV is attributed to $2p4h$ configuration while the 7^{+} level at 1784-keV appears to have a $1p3h$ configuration. The observed yrast 8^{+} and 9^{+} levels are well reproduced assuming both the $1p3h$ and $2p4h$ configurations. Thus one could conclude that the low-lying states have a pure configuration structure whereas levels above $E_x \sim 3$ MeV could have considerable configuration mixing.

In the present calculations, the model space was internally truncated to include the following $[\pi(f_{7/2})^{4-5},(p_{3/2})^{0-1},(f_{5/2})^{0-1},(p_{1/2})^{0-1}] \otimes [\nu(f_{7/2})^{7-8},(p_{3/2})^{0-1},(f_{5/2})^{0-1},(p_{1/2})^{0-1}]$ configurations. The calculated energy eigen values are compared with the experimental results in Fig. 5.23. It is observed that the low-lying levels in the shell-model up to a spin-parity of 9^{+} are in good agreement with the experimental ones. The present calculations could not reproduce the observed excitation energies for levels $J > 9^{+}$. A plausible explanation for this could be the truncation of the model space. The present calculations indicate that 8^{+} and 9^{+} levels are dominated by $1p3h$ configurations. We have also tried to perform the shell model calculations for the states above $J^{\pi} = 12^{+}$ by increasing the number of particles excited from the $f_{7/2}$ orbit.

However, due to computational limitations these calculations could not be performed for more than 4 particles excited from the $f_{7/2}$ orbit. These results indicated a lowering of the predicted excitation energies for the higher lying states. It is observed that the low-lying levels in the shell-model up to a spin-parity of 9^{+} are in good agreement with the experimental ones. The higher levels are not in good agreement with the present experimental levels, which may be due to truncation of the model-space. This is indicative of the dominance of a large number of intrinsic configurations for these states.

All the above calculations and detailed discussion are indicative of the dominance of a large number of intrinsic configurations for these states. The absence of any band-like sequences is indicative of the presence of single-particle behaviour up to the observed spins and excitation energy.

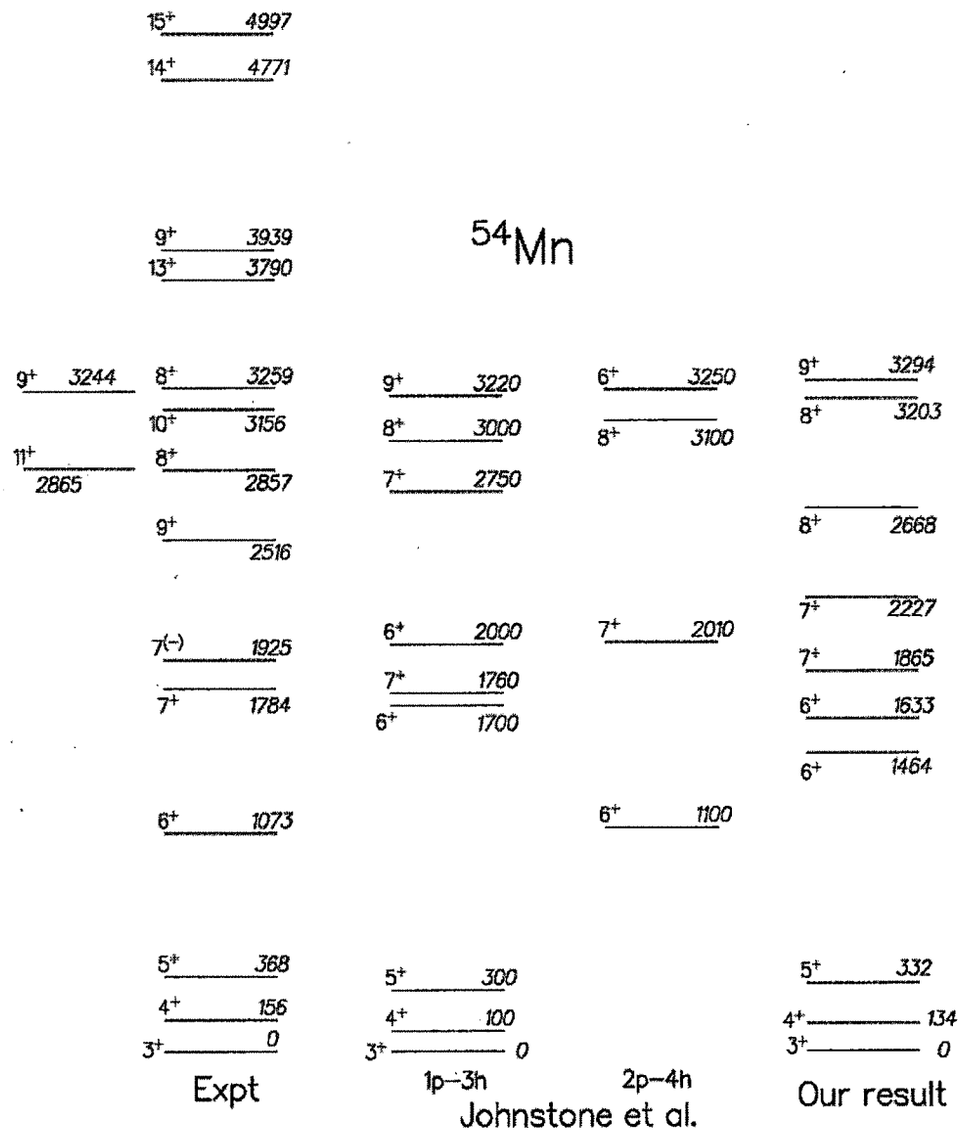

Figure 5.23: Comparison of the experimental levels of ^{54}Mn with the present predictions of the shell model calculations and Johnstone *et al.*, [39]; refer text for details.

5.7. Conclusions:

In the present work, the yrast energy levels in ^{36}Cl (Z = 17, N = 19) were populated *via* $^{20}Ne + ^{27}Al$ reaction at an incident energy of 145 MeV extending the level scheme to an excitation energy of 7.5 MeV. A six Clover array was used to detect the de-exciting γ-rays. The level scheme of ^{36}Cl is extended by adding more than fifteen new γ-transitions. These transitions were placed in accordance with the coincidence measurements. For this set of experimental analysis we could only perform the R_{DCO} calculations. DCO ratios and intensities measurements were obtained. Polarization calculation couldn't be performed due to less statistics in coincidence mode.

The level scheme of ^{54}Mn (Z = 25, N = 29) nucleus, in the reaction $^{20}Ne + ^{51}V$ have been populated up to $J = 15^+$ and $E_x \sim 5$ MeV. An eight Clover array was used to detect the de-exciting γ-rays. Nine new γ-transitions belonging to this nucleus have been identified and placed in the level scheme. Spin-parity assignments for most of the observed levels have been made unambiguously using the observed qualitative coincidence angular anisotropy and the coincidence linear polarization measurements. The level at E_x = 1925-keV appears to be a tentative negative-parity level, which is not apriori expected in these nuclei at such low excitation energies and this warrants further detailed experimental and theoretical investigations that are beyond the scope of present investigations.

The experimental results were compared with the results of the OXBASH shell model code with ^{40}Ca as the core. The results were in fair agreement with the theoretical ones in the lower excitation energies and vary in the higher side. These being an odd-odd nucleus, one expects the dominance of single-particle nature. Indeed, this is exhibited by irregular level spacing and many parallel decay branches and corroborated by the absence of any band-like structure. These nuclei at such low excitation energies have a complex level structure and this warrants further detailed experimental and theoretical investigations [51].

References

1. P. Baumann, *et al.,* Phys. Rev. C18, 2110 (1978)
2. A.S. Yousef, E.L. Sprenkel-Segel and R.E. Segel, Phys. Rev. C8, 684 (1973)
3. P.J. Nolan, *et al.,* J.Phys. G: Nucl. Phys. 2, 249 (1976)
4. P.J. Nolan, *et al.,* J.Phys. G: Nucl. Phys. 3, 10 (1977)
5. P.J. Nolan, *et al.,* J. Phys. A6, L37 (1973)
6. R. Sherr, *et al.,* Bull. Am. Phys. Soc. 19, 499 (1974); Phys. Lett. 52B, 401 (1974)
7. R.M. Del Vecchia, R.T. Kouzes and R. Sherr, Nucl. Phys. A265, 220 (1976)
8. H. Nann, W.S. Chein, A. Saha and B.H. Wildenthal, Phys. Rev. C15, 1959 (1977)
9. F.C. Erné, Nucl. Phys. 84, 91 (1966a); Nucl. Phys. 84, 241 (1966b)
10. J. Keinonen *et al,* Phys. Rec. C14, 160 (1976)
11. P.M. Endt and C. van der Leun, Nucl. Phys. A214, 1 (1973)
12. J.W. Olness, *et al.,* Phys. Rev. C11, 110 (1975)
13. E.K. Warburton, *et al.,* Phys. Rev. C14, 996 (1976)
14. R. Rascher, K.P. Lieb and M. Uhrmacher, in Sump. Nucl. Struc. Balatonfiired, Hungary, (Unpublished) (1975)
15. B. Krusche, *et al.,* Nucl. Phys. A386, 245 (1982)
16. A. Fubini, M. Popa, D. Prosperi and F. Terrasi, Nuovo Cim. 2A, 109 (1971)
17. A.M.J. Spits and J. Kopecky, Nucl. Phys. A264, 63 (1976)
18. M.L. Stelts and R.E. Chiren, Nucl. Instr. 155, 253 (1978)
19. T.J. Kennett, M.A. Islam and W.W. Prestwich, Can. J. Phys. 59, 93 (1981)
20. S. Piskor, P. Franc, W. Schaferlingova, J. Kremenek, Nucl. Phys. A481, 269 (1988)
21. C. Frießner, *et al.,* Phys. Rev. C 60, 011304 (1999)
22. S.M. Lenzi *et al.*, Phys. Rev. C 60, 021303 (1999)
23. C.E. Svensson *et al.*, Phys. Rev. C 58, R2621 (1998)
24. A. Schmidt, *et al.,* Phys. Rev. C 62, 044319 (2000)
25. Bao Guo Dong and HongChao Guo, Euro. Phys. J. A 17, 25-28 (1999)
26. M. Ogawa and H. Taketani, Nucl. Phys. A 194, 259 (1972)
27. P.G. Kerr, S.A. Wender and J.A. Cameron, Nucl. Phys. A 226, 381 (1974)
28. D.J. Beale, A.R. Poletti and J.R. Southon, Nucl. Phys. A 261, 238 (1976)
29. P. Beuzit, J. Delaunay, J.P. Fouan and H. Ronsin, Nucl. Phys. A 137, 97 (1969)
30. R.R. Betts, Ole Hansen, D.J. Pullen, Nucl. Phys. A 182, 69 (1972)

31. A.R. Majumder, H.M. Sen Gupta and A. Guichard, Nucl. Phys. A 209, 615 (1973)
32. A.R. Poletti, *et al.,* Phys. Rev. C 10, 2329 (1974)
33. A.M. Nathan, *et al.,* Phys. Rev. C 16, 192 (1977)
34. D.C. Radford and A.R. Poletti, J. Phys. G : Nucl. Phys. 5, 409 (1979)
35. M. Toulemonde, *et al.,* J. Phys. G : Nucl. Phys. 5, 819 (1979)
36. H. Horie and K. Ogawa, Prog. Theor. Phys. A 204, 561 (1973)
37. P.G. Kerr, S.A. Wender, J.A. Cameron, Nucl. Phys. A 226, 381 (1974)
38. A. Guichard, W. Benenson and H. Nann, Phys. Rec. C12, 1762 (1975)
39. I.P. Johnstone and H.G. Benson, J. Phys. G : Nucl. Phys. 3, L69 (1977)
40. G. Kiran Kumar et al., Proc. of DAE Symp. On Nucl. Phys., 51, 248 (2006), Proc. of the South African Inst. of Phys. Conf. (SAIP) (2006)
41. R. Raut *et al.*, Proc. of DAE Symp. On Nucl. Phys., 47B, 578 (2004)
42. D.C. Radford, Nucl. Inst. Meth. A361, 297 (1995)
43. N.S. Pattabiraman *et al.*, Nucl. Inst. Meth. A526, 432 & 439 (2004)
44. Krishichayan *et al.*, Eur. Phys. J. A 29, 151 (2006)
45. Krishichayan, 2007 Thesis submitted to the University of Calcutta, (Unpublished)
46. V. Avrigeanu, C. Bucurescu and G. Constaninescu, Nucl. Phys. A 272, 243 (1976)
47. L.R. Medsker, L.H. Fry Jr and D.C. Wilson, Phys. Rev. C 18, 2584 (1978)
48. W.D. Kampp, K.H. Bodenmiller, A. Nagel and S. Buhl, Z. Phys. A 288, 167 (1978)
49. G.A. Hoken, J.A.J. Hermans and A. Van Ginkel, Nucl. Phys. A211, 405 (1974)
50. B.A. Brown *et al.*, computer code OXBASH, (1984)
51. G. Kiran Kumar et al., J. of Phys. G: Nucl. and Part. Physics (In press) (2008)